Use of the Finite-Difference Time-Domain Method for Calculating EM Absorption in Man Models

DENNIS M. SULLIVAN, OM P. GANDHI, FELLOW, IEEE, AND ALLEN TAFLOVE, SENIOR MEMBER, IEEE

Abstract—**The finite-difference time-domain (FDTD) method is used to calculate the detailed specific absorption rate (SAR) within the human body. SAR distributions are calculated using incident frequencies of 100 and 350 MHz for three different cases: 1) a homogeneous man model in free space, 2) an inhomogeneous man model in free space, and 3) an inhomogeneous man model standing on a ground plane. These various cases are used to evaluate the advantage of inhomogeneous models over homogeneous models, and grounded models versus free space models. Finally, comparison is made between the results obtained here and those obtained experimentally or with the method of moments (MoM).**

I. Introduction

In a previous paper [1], the finite-difference time-domain (FDTD) method was introduced as a means of accurately calculating local specific absorption rates (SAR's) in human tissues. The method was described and test results using analytic methods to demonstrate accuracy were displayed. Finally, to demonstrate the ability of the *method to calculate SAR distribution in a large inhomo*geneous body, the SAR distribution of a 16 000 cell model of the human torso was calculated. At that time, it was also pointed out that the results were of dubious value, at least for E polarized incident radiation, because the torso was taken as an isolated body.

In this paper, we describe results obtained by using models of a complete man. The SAR's are computed for both homogeneous and inhomogeneous models in order to evaluate the advantages of using detailed inhomogeneous models. Since an isolated man standing in free space is not a very realistic assumption, an infinite conducting ground plane has been added to simulate a somewhat more realistic problem. The SAR distributions in these grounded models are then compared to the distributions obtained for models in free space. The above problems are run at two different frequencies, 100 and 350 MHz. The construction of the database is also briefly described, along with a description of the needed computer resources.

Manuscript received November 17, 1986; revised September 8, 1987. This work was supported by National Science Foundation Grant ECE 8303655 and by the National Institute of Environmental Health Sciences Grant ES 02304.

D. M. Sullivan and O. P. Gandhi are with the University of Utah, Salt Lake City, UT 84112.

A. Taflove is with the Department of Electrical Engineering and Computer Science, Northwestern University, Evanston, IL 60201.

IEEE Log Number 8718585.

II. Description of the Method

The FDTD method was first proposed by Yee [2] and later simplified by Taflove [3]. It is a direct implementation of the time dependent Maxwell's equations.

$$\frac{\partial D}{\partial t} + \boldsymbol{J} = \nabla \times \boldsymbol{H}, \qquad -\frac{\partial B}{\partial t} = \nabla \times \boldsymbol{E}. \tag{1}$$

The above vector equations are rewritten as six finite-difference equations for implementation on a computer. Taking the $\boldsymbol{E}$ and $\boldsymbol{H}$ equations in the z direction, for example,

$$\begin{aligned} EZ(I, J, K) = {} & CAZ(I, J, K) \times EZ(I, J, K) \\ & + CBZ(I, J, K) \times [HY(I, J, K) \\ & - HY(I-1, J, K) \\ & + HX(I, J-1, K) - HX(I, J, K)] \end{aligned} \tag{2a}$$

$$\begin{aligned} HZ(I, J, K) = {} & HZ(I, J, K) \\ & + DB \times [EX(I, J+1, K) \\ & - EX(I, J, K) \\ & + EY(I, J, K) - EY(I+1, J, K)]. \end{aligned} \tag{2b}$$

The method is implemented by generating a sinusoidal incident wave which propagates as the equations are solved. A model of the human body is generated by the electromagnetic properties, i.e., the dielectric constant and the conductivity, which are then used to calculate *CAZ* and *CBZ* (or *CAX* and *CBX* or *CAY* and *CBY* for the equations in the x or y direction, respectively) in (2a) above. Details of the method are given in [1].

III. Constraints and Limitations

In the FDTD method, the radiation condition is not implicit; i.e., the scattered waves must be truncated at the edge of the computing field. The truncation used is based on a two-pole expansion which, according to Bayliss and Turkel [4], results in an error on the order of the following expression.

$$\text{Error} \approx 0\left[\frac{c}{2\pi fr}\right]^{2.5} \tag{3}$$

0018-9294/88/0300-0179$01.00 © 1988 IEEE

where f is the incident frequency and r is the distance from the center of the scattering body to the edge of the computing field. (Details of the implementation are given in [5] and [6].) Equation (3) says that problems using lower incident frequencies may require a larger volume surrounding the body to avoid error due to imperfect truncation conditions.

To ensure stability, the time step is given by

$$\delta t = \frac{\delta}{2c} \tag{4}$$

where δt is the time step, δ is the cell size, and c is the speed of the electromagnetic wave. Equation (4) says that to use smaller cells, i.e., higher resolution, a proportionally smaller time step is necessary, and therefore a higher number of time steps will be required.

IV. Human Model

The model for the human body was taken from *A Cross-Section Anatomy* by Eycleshymer and Schoemaker [7]. This book contains cross-sectional diagrams of the human body which were obtained by making cross-sectional cuts at spacings of about one inch in human cadavers. The process is fully described in [1].

In this paper, we report on the SAR distribution using incident frequencies of 100 and 350 MHz. Two different man models are used for the two different frequencies. For 100 MHz, we use a model composed of 2.62 cm cubical cells. The entire man model resides in a rectangular volume with the dimensions 23 × 12 × 68 cells. For 350 MHz, we use 45 × 24 × 135, 1.31 cm cubical cells. Both represent a "standard man," 175 cm tall, weighing about 70 kg. Two separate models are needed for the following reasons: 1) the relative dielectric constants ϵ and conductivities σ for the various human tissues have different values at the different frequencies (see Table I) and 2) the two frequencies require different cell sizes. The reason for the two cell sizes is dictated by (3) and (4). At 350 MHz, a cell size of 1.31 cm is used. According to (3), the lower incident frequency at 100 MHz dictates a larger surrounding volume to avoid errors. Rather than use an enormous amount of computer resources, the cell size was increased to 2.62 cm. Of course, the price we pay for the larger cell size is loss of resolution.

V. Ground Plane

Since the SAR distribution of a man floating in free space is not a very realistic problem, the next logical step towards a practical situation is to add a ground plane under the man's feet. This would adequately simulate the SAR distribution of a man standing on high conductivity earth or any other grounded surface.

To accomplish this, we must now restrict ourselves to the case of incident waves which are propagating parallel to the ground plane and having an electric field polarized perpendicular to the ground plane. The implementation requires only two changes in the programs: first, the scattered field space below the total field space underneath the man's feet is removed, including the radiation boundary condition, so the feet of the man are right on the edge of the ground plane. The tangential E fields at this ground plane are set to zero and never changed. Second, the radiation boundary conditions around the rest of the space lattice must be changed slightly. In the free space model, we assumed, for the purpose of calculating the radiation condition, that the scattering was emanating from the center of the total field region. For the grounded model, we assume that the scattered field radiates from a point on the ground plane halfway between the man's legs.

This approach has been validated numerically for a grounded dielectric cylinder by comparing the SAR distribution against an ungrounded cylinder twice as long in free space. The two distributions agree to within 5 percent, as predicted by imaging theory.

TABLE I
Dielectric Constants and Conductivities for Human Tissues at 100 MHz and 350 MHz

	Organ	Dielectric Constant 100 MHz	Conductivity (S/m) 100 MHz	Dielectric Constant 350 MHz	Conductivity (S/m) 350 MHz
1.	Muscle	73.5	1.1	53.0	1.33
2.	Fat/bone	7.5	0.067	5.7	0.072
3.	Blood	74.0	1.1	65.0	1.2
4.	Intestine	36.2	0.55	26.5	0.66
5.	Cartilage	7.5	0.067	5.7	0.072
6.	Liver	77.0	0.62	50.0	0.82
7.	Kidney	90.0	1.01	53.0	1.16
8.	Pancreas	90.0	1.01	53.0	1.16
9.	Spleen	100.0	0.82	90.0	0.9
10.	Lung	75.0	1.03	35.0	1.1
11.	Heart	76.0	0.75	56.0	1.0
12.	Nerve	82.0	0.53	60.0	0.65
13.	Skin	24.5	0.55	17.6	0.44
14.	Eye	85.0	1.9	80.0	1.9

VI. Results

In this section, the results of using the FDTD method to compute SAR distributions in human models will be displayed. As mentioned earlier, six different cases will be reported:

1) homogeneous man model at 100 MHz
2) inhomogeneous man model at 100 MHz
3) grounded inhomogeneous man model at 100 MHz
4) homogeneous man model at 350 MHz
5) inhomogeneous man model at 350 MHz
6) grounded inhomogeneous man model at 350 MHz.

In each case, the illumination was an E-polarized plane wave incident on the front of the man model. We will use three methods to display the results:

1) a layer-by-layer average of the SAR distribution throughout the bodies
2) the average SAR distributions in selected organs.
3) contour diagrams of the SAR distributions of selected cross sections of the bodies.

The layer averages in item 1) are computed by adding all the SAR values on one level in the z direction (the axis of the man model) and dividing by the number of points within the body on that level. The SAR distributions within the organs in item 2) are calculated by simply averaging the SAR values within various regions in the body. For the most part, these regions represent only a small rectangular volume within the respective organ. (Rectangles are used so that area can be identified easily.) These volumes vary from two points for eyes (in this case, the two points that represent the locations of the eyes) to 160 points for the 350 MHz model of the liver. The wrist, knee, and ankle SAR's are calculated by using all the points in the respective level of the limb. Results are given in Table II. Finally, we show a group of contour diagrams which demonstrate the ability of the FDTD method to determine a high resolution of SAR distribution.

Figs. 1 and 2 show the layer-averaged SAR profiles. A mass density ρ of 10^3 kg/m^3 is assumed for the tissues to convert the energy absorbed per unit volume σE^2 to SAR's. Note that this is not a true SAR since SAR $= \sigma E^2/\rho$. We are using the absorbed power per unit volume σE^2 since our model does not allow for variations in ρ at the present time. In bone and in tissues such as lung, this could be substantially different than the SAR, and in the future, better models will be used. However, for the sake of simplicity, this quantity will be referred to as SAR in this paper. Notice that the basic shape of the profiles is determined mainly by the geometry; i.e., narrow sections such as neck and ankles have the highest SAR averages. The reason is the higher current densities for smaller cross-sectional dimensions and resulting higher SAR's. However, the relative magnitudes change as we go from homogeneous to inhomogeneous, or ungrounded to grounded models. And the effects are clearly more pronounced at 100 MHz than 350 MHz. At 100 MHz, for instance, the peak that occurs at 50 cm (at about the knee) is much higher when the inhomogeneous model is used. And when the model is grounded, the SAR's in the lower part of the body are severely affected. In contrast, at 350 MHz there is not much difference in the shape of the profiles. Grounding the model affects the average SAR's in the lower legs, but not much elsewhere.

Table II gives the SAR's in various organs for all three cases at both 100 and 350 MHz. Here it can be seen that even when there is not much difference in the layer-averaged SAR's, there can be significant differences in the internal SAR distributions. For instance, at 350 MHz there is not much difference in the shape of the homogeneous and inhomogeneous profiles. But Table II shows significant differences in the absorptions that occur in the brain, heart, and knee. Similarly, in the 350 MHz example, there is no energy absorption in the kidneys, while in the 100 MHz examples there are small but not insignificant amounts. This is due to the fact that the higher rate of energy absorption for a high frequency does not allow much energy to penetrate to an organ that is located towards the back of the body. We can also notice that

TABLE II
AVERAGE SAR'S WITHIN VARIOUS ORGANS IN THE BODY

	100 MHz			
Organ	Number of points	Homogeneous mW/kg	Inhomogeneous mW/kg	Grounded mW/kg
Brain	12	39.9	43.3	62.9
Eyes	2	62.0	56.0	86.5
Lung	12	30.4	51.5	71.2
Heart	4	29.9	40.8	53.6
Liver	12	25.6	33.8	44.4
Kidney	2	21.4	31.6	18.4
Wrist	21	324.0	350.0	226.0
Knee	51	238.0	470.0	298.0
Ankle	38	99.0	152.0	469.0
Whole Body	5,889	107.7	116.0	105.8

	350 MHz			
Organ	Number of points	Homogeneous mW/kg	Inhomogeneous mW/kg	Grounded mW/kg
Brain	96	38.5	77.4	77.6
Eyes	2	104.0	189.0	182.0
Lung	60	9.6	14.7	14.9
Heart	60	13.9	26.5	29.3
Liver	120	16.4	24.0	26.9
Kidney	12	0.	0.	0.
Wrist	59	238.0	227.0	246.0
Knee	161	61.6	99.8	98.4
Ankle	115	100.0	98.4	125.0
Whole body	40,067	56.39	56.59	58.47

gounding the model has little effect on the SAR's in organs in the upper half of the body at 350 MHz. At 100 MHz, we see that there is not only substantial differences between homogeneous and inhomogeneous SAR's, but that grounding the model has an effect on absorption throughout the body.

Lastly, we show some contour diagrams to illustrate the SAR distributions at various levels for the different models. Fig. 3(a) and (b) shows SAR distributions through the head at eye level for homogeneous and inhomogeneous models at 350 MHz, respectively. Note the homogeneous model misses the peaks that occur at the eyes, and a relative "hot spot" that occurs in the middle of the brain. These features are both missing in the homogeneous model. Fig. 4(a) and (b) shows contour plots of a level containing the kidneys and liver for homogeneous and inhomogeneous models at 100 MHz. Here the results are less dramatic, but still substantial. Notice that although the shapes of the contours are not radically different, the values through vital organs are.

VII. COMPARISON TO OTHER METHODS

In order to verify the results given here, a comparison was made with the experimental results of Stuchly and his associates [8]. This comparison was made using the 350 MHz man model. Stuchly uses a model composed of a viscous fluid which has the electrical properties of about

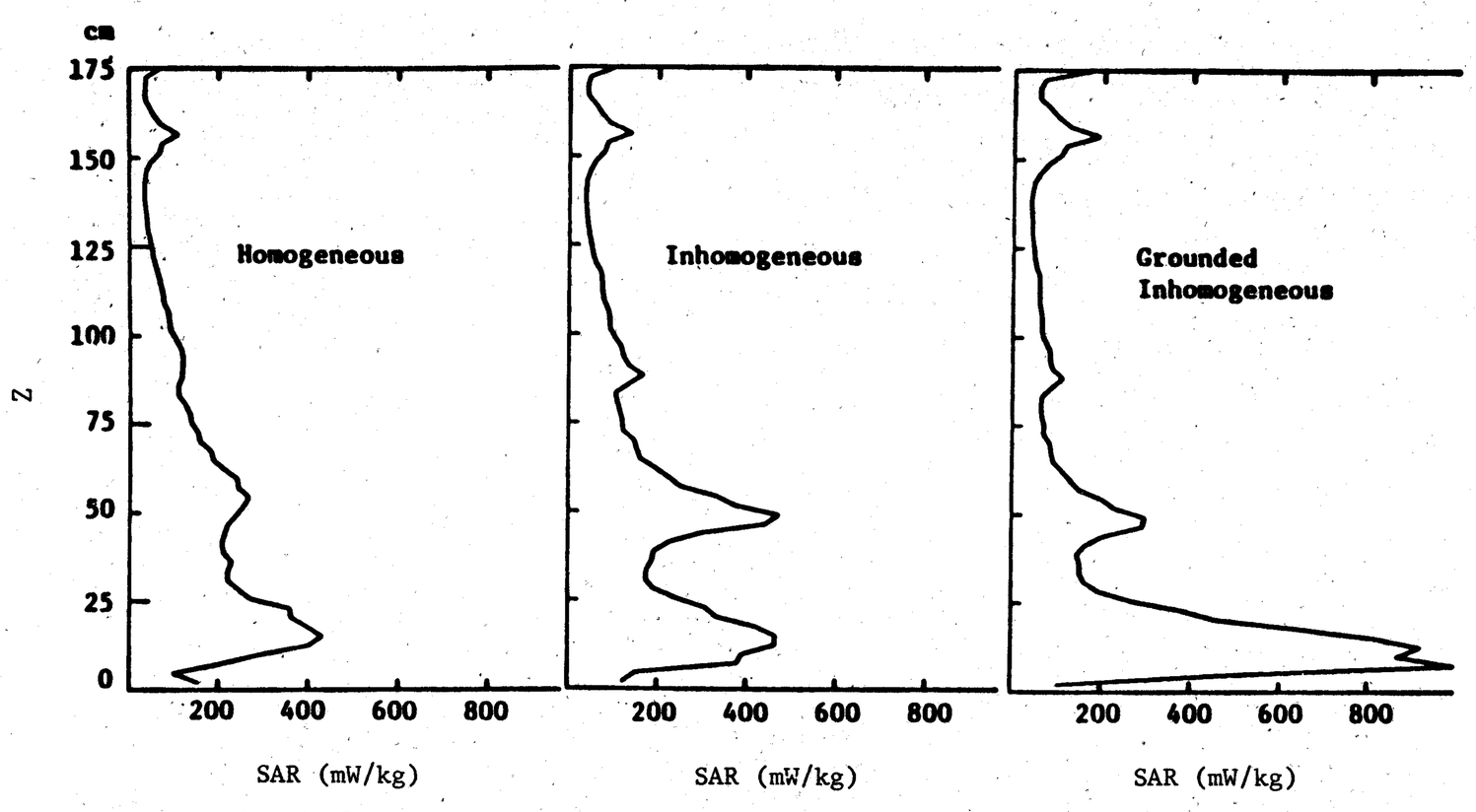

Fig. 1. Layer-averaged SAR distributions for man models at 100 MHz. All SAR's are the result of 1 mW/cm^2 incident wave.

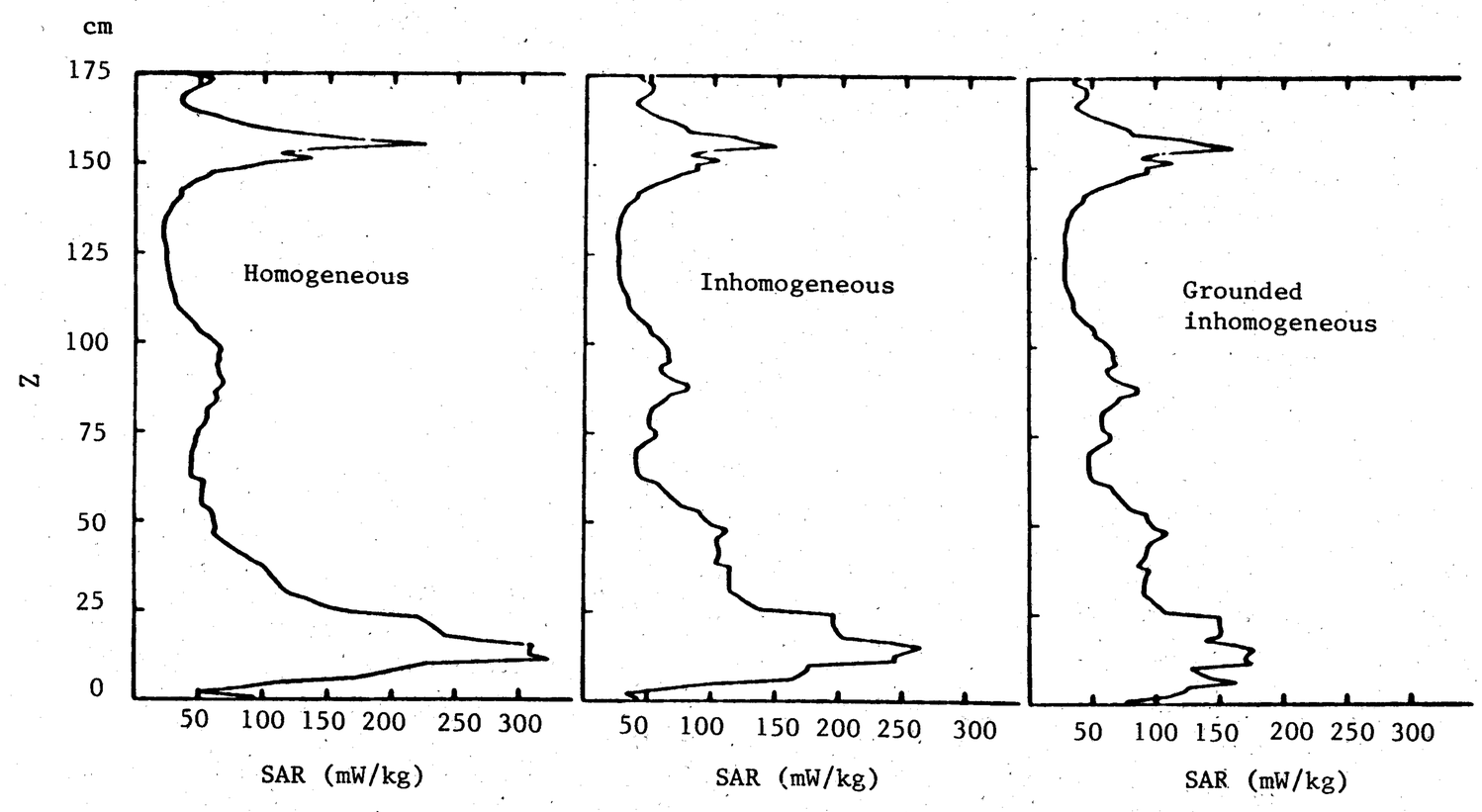

Fig. 2. Layer-averaged SAR distributions for man models at 350 MHz. All SAR's are the result of 1 mW/cm^2.

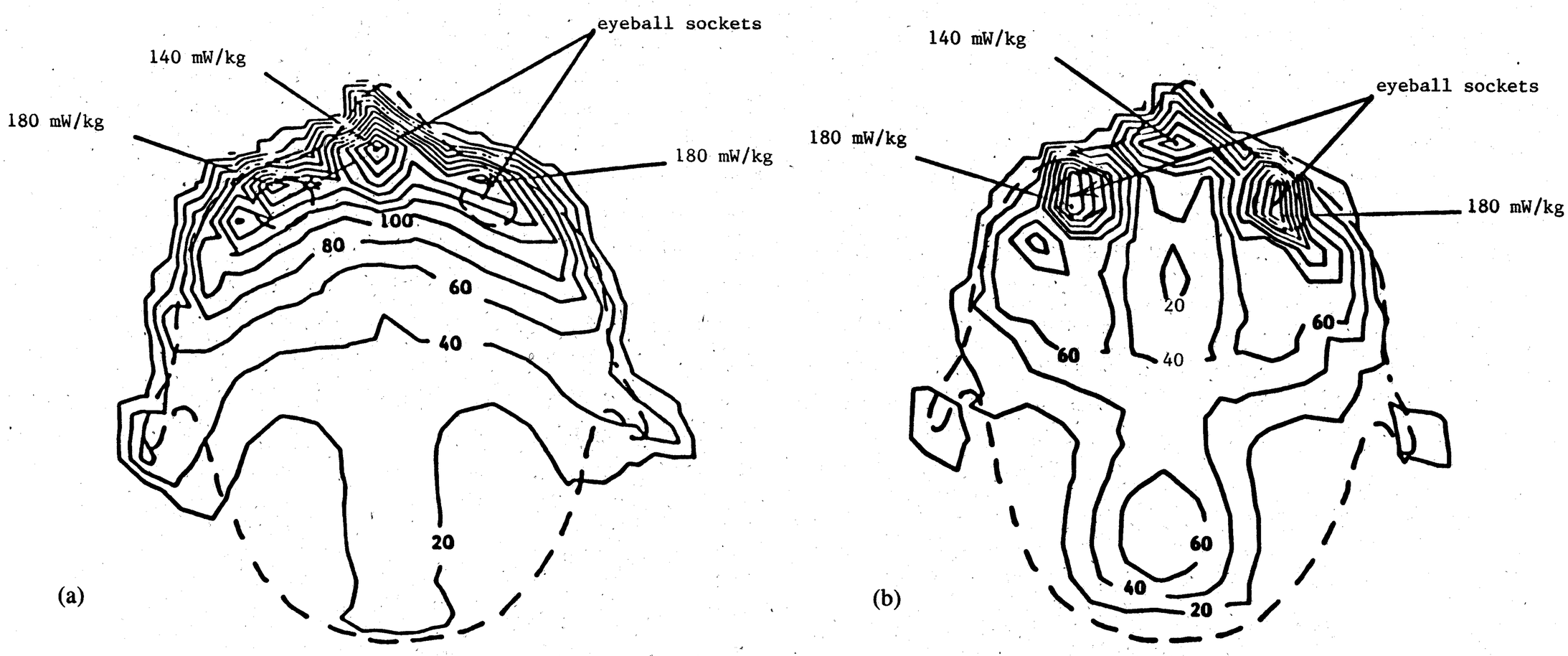

Fig. 3. (a) Contour diagram of the SAR distribution through the head of a homogeneous man model. Incident plane wave was 1 mW/cm^2 at 350 MHz. Each contour is 20 mW/kg. (b) Contour diagram of the SAR distribution through the head of an inhomogeneous man model. Incident plane wave was 1 mW/cm^2 at 350 MHz. Each contour is 20 mW/kg.

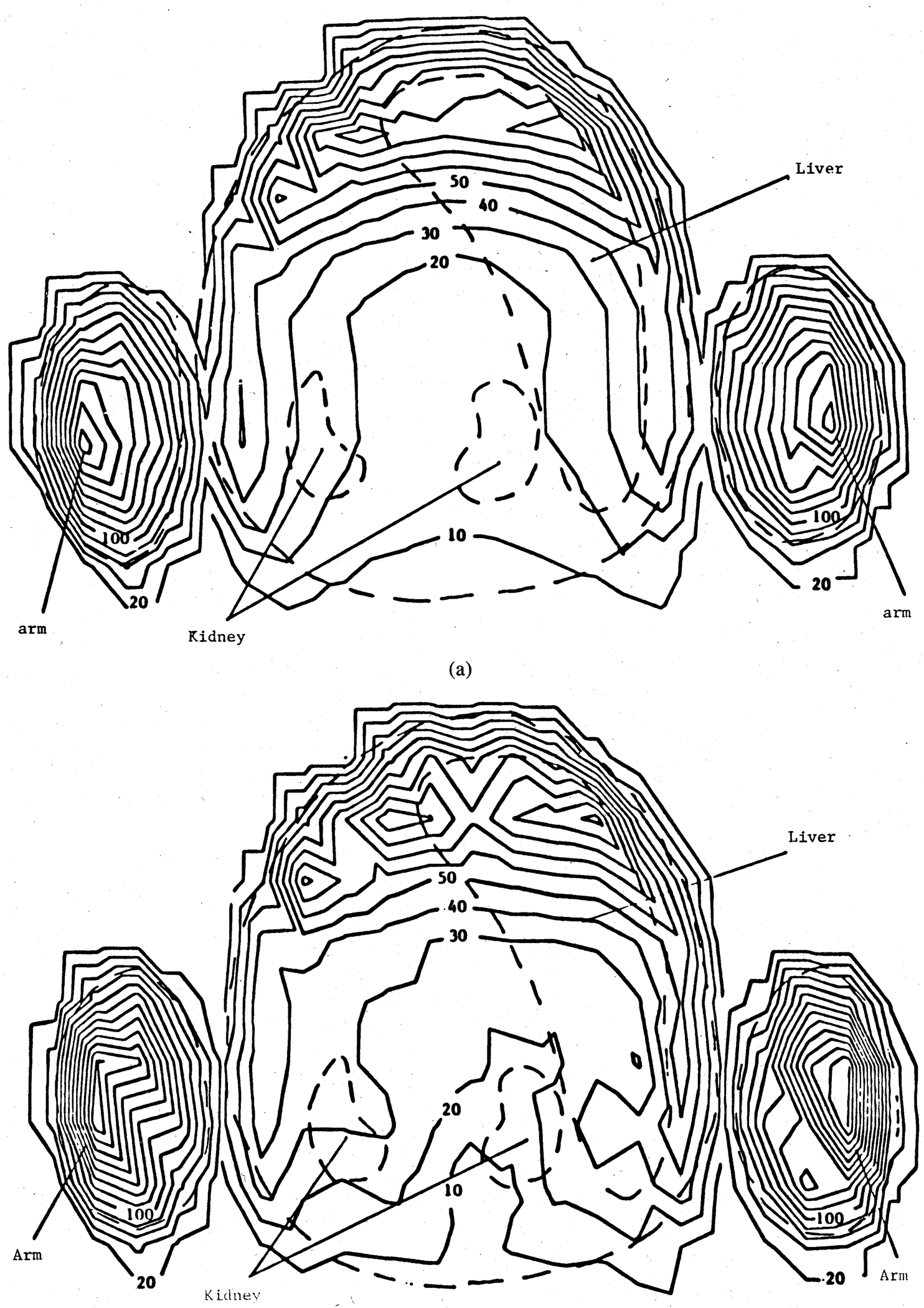

Fig. 4. (a) Contour diagram of the SAR distribution through the liver of a homogeneous man model. Incident plane wave was 1 mW/cm^2 at 100 MHz. Each contour is 20 mW/kg in the arms but 10 mW/kg in the body. (b) Contour diagram of the SAR distribution through the liver of an inhomogeneous man model. Incident plane wave was 1 mW/cm^2 at 100 MHz. Each contour is 20 mW/kg in the arms but 10 mW/kg in the body.

two-thirds muscle tissue ($\epsilon_r = 38$, $\sigma = 0.95$ S/m). The experiments were performed utilizing implantable nonperturbing electric field probes and a computer-controlled scanning system to measure SAR's in the model, which is irradiated by antennas located at sufficiently large distances to produce far-field exposure conditions. The layer-averaged SAR's are compared to those of the FDTD method of Fig. 5.

Although the basic shapes that the two methods present are the same, the magnitudes through the torso region are substantially different by greater than 2:1 variation in many places. And the whole body averages are somewhat different: 40.7 mW/kg for the experimental results versus 56.4 mW/kg for the FDTD. However, a couple of points should be remembered. First, Stuchly reports a 25 percent uncertainty in determining the SAR averages for the experimental model. Based on the results in evaluating the FDTD against analytic results, an uncertainty of

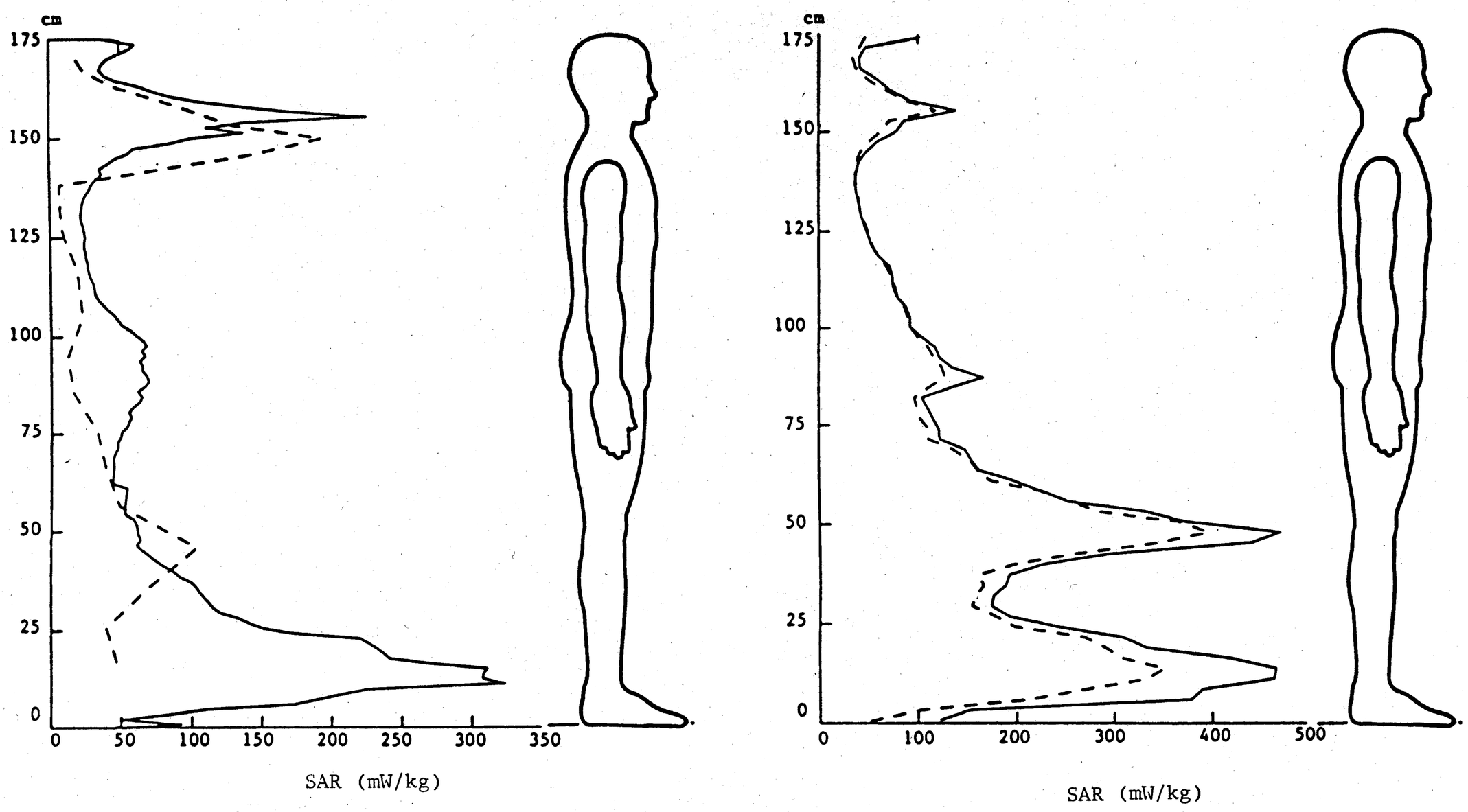

(a)

Fig. 5. Comparison of layer-average SAR's for experimental data [8] (dashed line) versus FDTD data (solid line) at 350 MHz. In both cases, a homogeneous model with $\epsilon_r = 38$ and $\sigma = 0.95$ S/m which represents a "standard man" of 175 cm and 70 kg is used. Whole body average is 40.7 mW/kg for the experimental method versus 56.4 mW/kg for FDTD.

12 percent should be allowed in estimating whole body averages [1]. These uncertainty ranges could, at least mathematically, account for the discrepancy. But there is a more plausible explanation. Even though each method employed a model of the same height and weight, they did not use exactly the same model.

A much better correlation was obtained when comparing the inhomogeneous 100 MHz SAR distribution of the FDTD method with one obtained using method of moments (MoM) [9]. Results are shown in Fig. 6(a) and (b) [10]. Fig. 6(a) is a comparison of free space inhomogeneous man models at 100 MHz and Fig. 6(b) is a comparison of inhomogeneous grounded man models at 100 MHz. Not only are the profiles very close, but the whole-body-averaged SAR's are also close: 116.0 mW/kg for FDTD versus 101.4 mW/kg for MoM for free space; 105.8 mW/kg for FDTD versus 93.0 for MoM for the grounded case. For these comparisons, however, the same model was used for both methods.

VIII. Conclusions

The FDTD method has been shown to be capable of calculating detailed SAR distributions for human models. The strength of this method is the fact that computer resources increase only linearly with the number of cells used in the model. And with supercomputers, such as the CRAY II, models of 40 000 cells are possible. However, a drawback of this method is the limitation of frequency

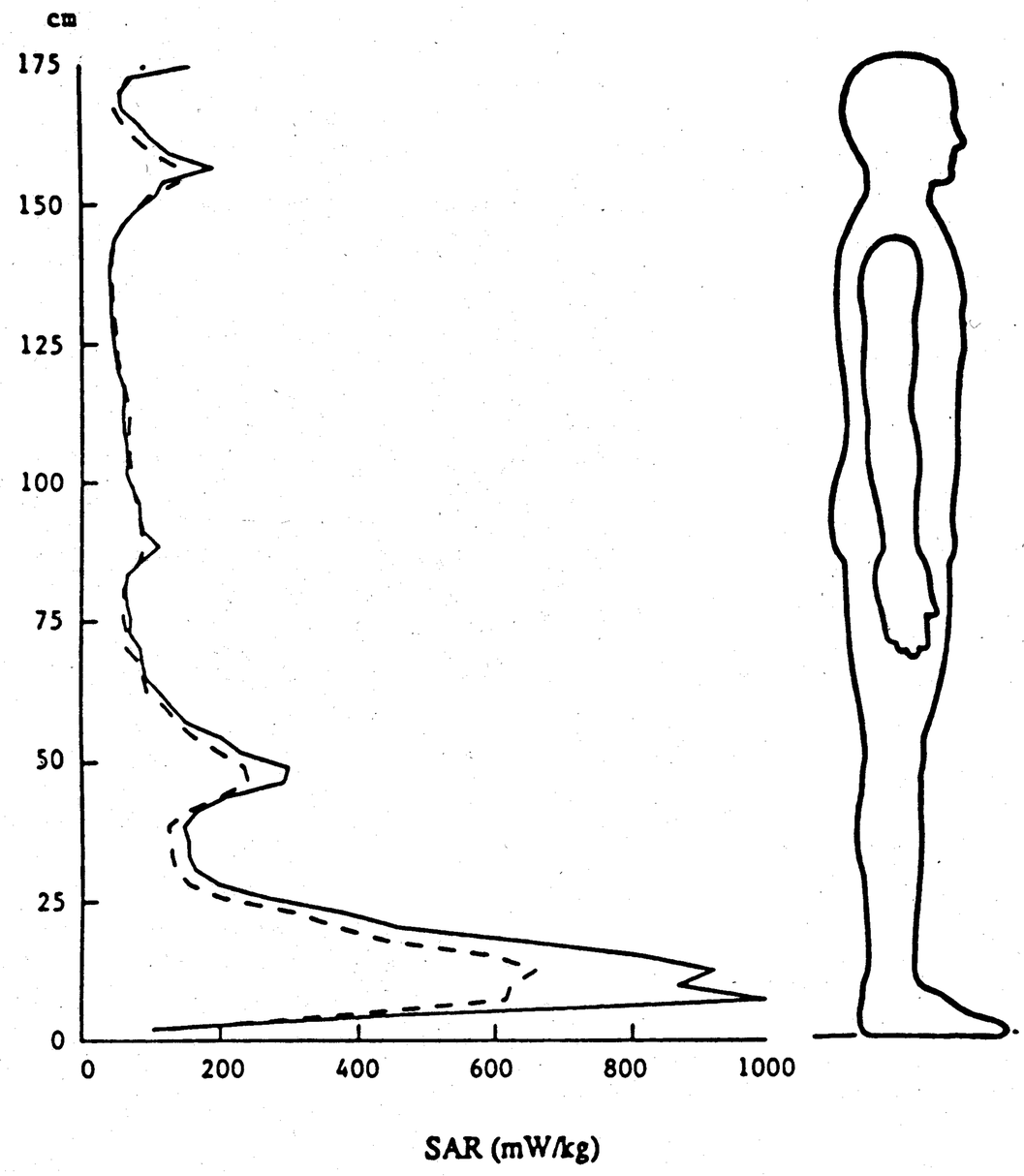

(b)

Fig. 6. Comparison of layer-averaged SAR's as determined by method of moments [10] (dashed line) versus FDTD data (solid line) at 100 MHz. In both cases, an inhomogeneous model representing a "standard man of 175 cm and 70 kg is used. (a) Free-space model. Whole body average is 101.4 mW/kg via MoM versus 116.0 via FDTD. (b) Grounded-model. Whole body average is 93.0 mW/kg via MoM versus 105.8 via FDTD.

range for a given cell size. At the present time, use of frequencies less than 50 MHz or greater than 700 MHz would put a strain on computer resources. As explained in Section III, low frequencies require more time steps and a larger total space. Higher frequencies would need a very small cell size, which would require an inordinately large number of cells for the man model.

Some comparisons of inhomogeneous versus homogeneous, and grounded versus ungrounded, models have also been presented. It is shown that homogeneous models are capable of determining total SAR's or even layer-averaged SAR's for man models, but cannot give the correct SAR distribution through internal organs. It is further shown that the SAR distribution of an ungrounded model does not vary significantly from that of the grounded model at 350 MHz, but does so at 100 MHz.

At the present time, the biggest drawback to the FDTD method is the constraints described in Section III and illustrated in Section IV. These constraints imply that given a certain cell size, there is a limited band of frequencies at which a problem can be accurately and economically run. Equation (3) puts an upper limit on the frequencies for which accuracy can be expected. Frequency-dependent error due to the radiation boundary condition, along with the need for more time steps at lower frequencies (4), place a limit on the lower frequency due to the need for additional computer resources.

An obvious possibility for extending the lower range is higher order radiation boundary conditions. For instance, if we were to use three-pole expansion instead of only two, which we are presently using, then the error term in (3) would be raised to the 3.5 power instead of 2.5. This would give a substantially smaller error at any given frequency f, so we could afford a substantially larger r (i.e., a smaller scattered field) which would cut down computation time considerably. For instance, we could run the 100 MHz incidence on the 1.31 cm man model for only about three times the cost of the 350 MHz incidence rather than six times the cost. Such improved boundary conditions are being developed.

Even though we now have a detailed inhomogeneous model of a man standing on a grounded surface, we are still restricted to the case of the incident plane waves. A major extension would be the ability to generate arbitrary near-field sources. This may be possible by actually modeling the generator within the space, i.e., model the generator according to its dielectric constant and conductivity, and then assign it E-field values, similar to the way an antenna is stimulated by applying a voltage. Conceptually, the coupling to the surrounding air would result in the appropriate incident field.

REFERENCES

[1] D. M. Sullivan, D. T. Borup, and O. P. Gandhi, "Use of the finite-difference time-domain method in calculating absorption in human tissues," *IEEE Trans. Biomed. Eng.*, vol. BME-34, pp. 148–157, Feb. 1987.

[2] K. S. Yee, "Numerical solution of initial boundary value problems involving Maxwell's equations in isotropic media," *IEEE Trans. Antennas Propagat.*, vol. AP-14, pp. 585–589, 1966.

[3] A. Taflove and M. E. Brodwin, "Computation of the electromagnetic fields and induced temperatures within a model of the microwave-irradiated human eye," *IEEE Trans. Microwave Theory Tech.*, vol. MTT-23, pp. 888–896, Nov. 1975.

[4] A. Bayliss and E. Turkel, "Radiation boundary conditions for wave-like equations," *Commun. Pure Appl. Math.*, vol. 33, pp. 707–725, 1980.

[5] G. Mur, "Absorbing boundary conditions of the finite-difference approximation of the time-domain electromagnetic field equations," *IEEE Trans. Electromagn. Compat.*, vol. EMC-23, pp. 377–382, 1981.

[6] K. Umashankar and A, Taflove, "A novel method to analyze electromagnetic scattering of complex objects," *IEEE Trans. Electromagn. Compat.*, vol. EMC-24, pp. 433–439, 1983.

[7] A. C. Eycleshymer and D. M. Schoemaker, *A Cross-Section Anatomy*. New York: Appleton, 1911.

[8] S. S. Stuchly, M. A. Stuchly, A. Draszelqski, and G. Hartsgrove, "Energy deposition in a model of man: Frequency effects," *IEEE Trans. Biomed. Eng.*, vol. BME-33, pp. 702–711, 1986.

[9] D. T. Borup and O. P. Gandhi, "Fast-Fourier-transform method for calculation of SAR distributions in finely discretized inhomogeneous models of biological bodies," *IEEE Trans. Microwave Theory Tech.*, vol. MTT-32, pp. 355–360, Apr. 1984.

[10] D. T. Borup, personal communication.

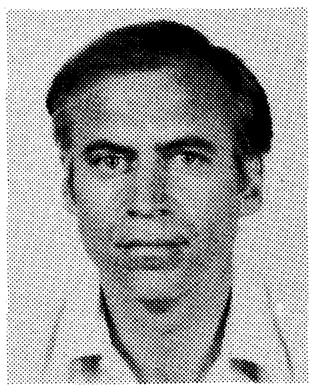

Dennis M. Sullivan was born in Madison, WI, on January 3, 1949. He received the B.S.E.E. degree from the University of Illinois in 1973, and the M.A. degrees in electrical engineering and computer science from the University of Utah in 1978 and 1980, respectively, and completed his Ph.D. studies in electrical engineering at the University of Utah, Salt Lake City, in 1987.

Between May 1981 and December 1981, he worked at the University of Utah Research Institute using ultrasound in sensory feedback applications, and tested and evaluated medical devices. His doctoral thesis was the development of computer software to determine electromagnetic energy absorption in humans exposed to microwave fields. He has recently returned from Europe where he worked as a development engineer for Bopp and Reuther, Mannheim, West Germany. He is currently a Research Engineer at the Stanford Medical Center, Stanford, CA.

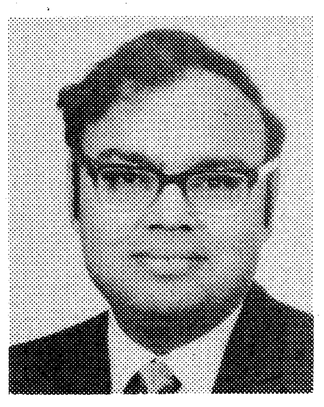

Om P. Gandhi (S'57–M'58–SM'65–F'79) received the B.Sc. (Honors) degree in physics from Delhi University, Delhi, India, and the M.S.E. and Sc.D. degrees in electrical engineering from University of Michigan, Ann Arbor.

He is a Professor of Electrical Engineering at the University of Utah, Salt Lake City. He is an author or coauthor of one technical book and over 180 journal articles on microwave tubes, solid-state devices, and electromagnetic dosimetry and has recently written the textbook *Microwave Engineering and Applications* (New York: Pergamon). He has been a principal investigator on over two dozen federally-funded research projects since 1974 and serves or has served as a consultant to several government agencies and private industries.

Dr. Gandhi received the Distinguished Research award of the University of Utah for 1979–1980 and a special award for "Outstanding Technical Achievement" from the Institute of Electrical and Electronics Engineers, Utah Section, in 1975. He is a past Chairman of the IEEE Committee on Man and Radiation (COMAR). His name is listed in *Who's Who in America*, *Who's Who in Engineering*, and *Who's Who in Technology Today*.

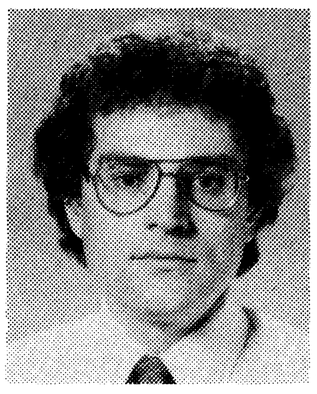

Allen Taflove (M'75–SM'84) was born in Chicago, IL on June 14, 1949. He received the B.S., M.S., and Ph.D. degrees in electrical engineering from Northwestern University, Evanston, IL, in 1971, 1972, and 1975, respectively.

From 1975 to 1984, he was a staff member at IIT Research Institute, Chicago, IL, holding the positions of Associate Engineer, Research Engineer, and Senior Engineer. His research there was concerned with electromagnetic wave penetration and scattering, power-frequency coupling of earth-return transmission systems, and development of novel techniques for recovery of oil from shale, tar sand, and conventional wells based upon *in situ* radio frequency heating. He was principal investigator on eight externally funded programs in these areas, including five programs which contributed to the early development of the finite-difference time-domain numerical modeling approach for complex electromagnetic wave interaction problems. In 1984 he joined the Department of Electrical Engineering and Computer Science Northwestern University, Evanston, IL, as an Associate Professor. Since then, he has developed several research programs in the area of computational electromagnetics. His current research interests include applications of recent supercomputers, wave penetration and scattering by large, complex structures, inverse scattering/target synthesis, and the new on-surface radiation condition theory.

Dr. Taflove is a member of Commission B of URSI, Eta Kappa Nu, Tau Beta Pi, Sigma Xi, AAAS, and the New York Academy of Sciences. He has been granted ten U.S. patents for his *in situ* oil recovery inventions, and was senior author of a paper awarded in the Best Paper prize at the IEEE 1983 International Symposium on Electromagnetic Compatibility, Washington, DC.